Facet growth kinetics and diameter fluctuations in molten zone Si crystal growth

Christian Kranert, Paul Wimmer, Jochen Friedrich, Thierry Duffar

Journal of Crystal Growth 652 (2025) 128024

Contents lists available at ScienceDirect

Journal of Crystal Growth

journal homepage: www.elsevier.com/locate/jcrysgro

Facet growth kinetics and diameter fluctuations in molten zone Si crystal growth

Christian Kranert [a,*], Paul Wimmer [a], Jochen Friedrich [a], Thierry Duffar [a,b]

[a] Fraunhofer IISB, Schottkystrasse 10, 91058 Erlangen, Germany
[b] University Grenoble Alpes/Grenoble INP, CNRS, SIMAP, Grenoble, France

ARTICLE INFO

Communicated by Chung wen Lan

Keywords:
Silicon
Solid-liquid interface
Facets
Growth kinetics
Dislocations

ABSTRACT

Several <111> oriented silicon single crystals have been grown in ellipsoid mirror furnaces at various growth rates by the zone melting technique. The crystals grown with initial necking show no dislocation and large (111) facets perpendicular to the growth axis. Measurements of facet growth rate and undercooling allowed selecting the applicable kinetic coefficients in case of facets growing through 2D-seed nucleation mode. Crystals grown without necking exhibit dislocations and show smaller stable facets, allowing the determination of the kinetic coefficient in case of dislocation-driven facet growth. Among these crystals, those grown at lower velocity, with a lower temperature gradient, show a decrease of dislocation density with length of the crystal and an increase of facet diameter fluctuations. A geometric model of dislocation-facet interaction suggests that these diameter fluctuations are due to the effect of individual dislocations crossing the facet, which increase when the dislocation density decreases.

1. Introduction

The occurrence of a facetted solid–liquid interface during melt growth of oxides and semiconductor crystals is a very common phenomenon in crystal growth. For III-V semiconductors, facets are frequently associated with the formation of other crystal defects like twins (see e.g. [1–5]). The presence of so-called edge facets in Czochralski and Floating Zone growth of silicon crystals is an indicator for a dislocation free growth process as the growth kinetics of facets and therefore its size depends on the presence of dislocations. However, there are only few publications in which the impact of the kinetics of the solid–liquid interface on the final crystal morphology and defects (dislocations, twins, grain boundaries …) was studied [6–12], especially in the case of a facetted solidification interface during silicon crystal growth. On the fundamental point of view, because silicon is a monoatomic material with well-known properties, it is actually a good candidate for such kind of analyses.

According to the Jackson's criterion [13] and confirmed by many experiments, facets in silicon are always {111} planes. In order to grow at a given growth rate V, facets need an undercooling ΔT which depends on the atomic piling at the facet-liquid interface. Three facet growth mechanisms exist in the case of Si, each associated to a specific V-ΔT kinetic law:

- 2D-seed nucleation on the facet surface occurs when there is no interaction with a dislocation. This phenomenon requires high undercooling. The 2D-seed provides a step on the facet surface, which expands laterally, resulting in an additional solidified atomic layer. Through theoretical considerations and comparison with experimental results, Voronkov [14] obtained the relation:

$$V_{0D} = 63000{*}\Delta T^{\frac{5}{6}}{*}e^{\frac{-44.4}{\Delta T}}\left(1.66{*}10^{-4}(1683-\Delta T)^2\right)^{\frac{1}{6}}\left(V\text{in }\mu\text{m.s}^{-1}\right), \quad (1)$$

leading to undercooling ΔT of the order of 3.5 K at usual growth rates. Beattie [15] performed Monte Carlo simulation of Si (111) facet growth and obtained:

$$V_{0D} = 226220{*}\Delta T^{\frac{2}{3}}{*}e^{\frac{-46.67}{\Delta T}}\left(V\text{in }\mu\text{m.s}^{-1}\right) \quad (2)$$

with undercooling ΔT larger than 4 K. Molecular dynamic simulations, performed by Fabiyi [16] gave the following relation with smaller undercooling ΔT of the order of 1.5 K:

* Corresponding author.
E-mail address: christian.kranert@iisb.fraunhofer.de (C. Kranert).

https://doi.org/10.1016/j.jcrysgro.2024.128024
Received 21 October 2024; Received in revised form 20 November 2024; Accepted 27 November 2024
Available online 11 December 2024

$$V_{0D} = 342000^{*}\Delta T^{\frac{2}{3}}{}^{*}e^{\frac{-14.64}{\Delta T}} \left(V \text{in } \mu\text{m.s}^{-1}\right). \quad (3)$$

- When a dislocation impinges on the facet, it generates a step on the interface that expands laterally in a spiral way [17]. As there is no more need for a surface seed, the undercooling is much lower, some 0.1 K, with a typical parabolic kinetic law:

$$V_{Dislo} = k_D \Delta T^2 \left(V \text{in } \mu\text{m.s}^{-1}\right), \quad (4)$$

  Through experiments, Voronkov [14] obtained the kinetic coefficient:$k_D = 300$ μm.s^{-1}.K^{-2}, while other experiments [18] suggested $k_D = 1000$ μm.s^{-1}.K^{-2}.
- In-situ undercooling measurements of facets occurring at grain boundaries [19] have shown that they were vicinal to {111} planes, i.e. growing through a continuous flow of steps. However, the origin of the steps, either from the grain boundary side of the facet or from the facet-rough interface junction, remains unknown. Molecular dynamic simulations [20] provided the kinetic law for vicinal facets of Si grown from the melt:

$$V_{\text{vicinal}} = \frac{0.3}{l(\text{nm})} 700000^{*}\Delta T \left(V \text{in } \mu\text{m.s}^{-1}\right), \quad (5)$$

  where l is the length of the terraces separating the steps.

In parallel to these well understood mechanisms, experimental measurements of undercooling versus velocity during growth, are scarce and gave dispersed results, spanning between 0.1 K and several K depending on the growth mechanism [21], so that it is difficult to decide which kinetic law coefficients should be used. This is important from a practical point of view. For example, Bagheri-Sadeghi and colleagues have shown that an accurate value of the 2D nucleation kinetic coefficient is mandatory for a better control of the horizontal ribbon growth of Si [22].

In this work a series of heavily As-doped, <111>-oriented silicon crystals with a diameter of 8 mm were grown by the Floating Zone (FZ) and Zone Melting (ZM) techniques [23]. Transverse cuts of the obtained samples have shown, as expected, {111} central facets along the crystals. The behavior of the central facet in dependence on the growth velocity and the presence of dislocations was studied by X-ray topography and optical microscopy on etched longitudinal samples cut from the crystals. The objective of this paper is to present and discuss the occurrence, behavior and kinetics of these facets, without and with dislocation interaction.

2. Experiments

Floating Zone (FZ) experiments in a double ellipsoid mirror furnace [24,25] and Zone Melting (ZM) experiments in a mono ellipsoid mirror furnace [26] were performed using single crystalline, heavily As-doped ([As] = 2.5x10^{19} at/cm^{-3}; resistivity = 2.5–3.0 mΩ cm), <111> -oriented silicon rods with 8 mm diameter and a length of 80–100 mm. At the beginning of the crystal growth process a molten zone with a zone height of 10–12 mm was established in the lower part of the sample. The molten zone was moved through the silicon rod at constant pulling speed V of 16.6, 33.3, 50, and 83.3 μm.s^{-1} (1 to 5 mm min^{-1}). During the growth process, the power of the lamp heater was adjusted manually to keep the zone height nearly constant. At the end of the growth process, the lamp power was decreased and then shut off to let the crystal cool down. The grown crystal length varied between 25 to 60 mm.

During the growth process the sample was rotated at a constant rotation rate of 10 rpm (FZ experiments) and 12 rpm (ZM experiments), respectively, to intentionally generate rotational striations for the determination of the growth velocity.

The experiments in the double ellipsoid mirror furnace were carried out by the Floating Zone technique, i.e. with a free surface of the liquid zone. This configuration allows to grow a Dash-Neck [27] by adjusting the lamp power and the pulling speed at the beginning of the growth process. The Dash necking procedure applied here has proven to grow dislocation free crystals [23]. Fig. 1 (top) shows a silicon crystal with a neck grown by the FZ technique in the present work.

The experiments in the mono ellipsoid mirror furnace were carried out by the Zone Melting method by using an oxidized silicon rod having a 5 μm thick SiO_2 skin on its surface to avoid Marangoni convection [28]. In this configuration, no necking procedure can be carried out and the crystals are dislocated [23]. The thermal conditions for the ZM experiments in the mono ellipsoid mirror furnace depend on the pulling rate. It was found experimentally and by numerical simulations [23,29] that the axial temperature gradient in the solid silicon is increasing from around 150 K cm^{-1} at a pulling rate of 16.6 μm.s^{-1} to more than 300 K cm^{-1} at 83.3 μm.s^{-1}. It is assumed that the thermal conditions are similar for the FZ experiments in the double ellipsoid mirror furnace. A typical silicon crystal grown by the Zone Melting technique is shown in Fig. 1. More details about the experimental procedure can be found in [23,30].

From the grown crystals one or two slices (1–2 mm thick) were cut from the middle parallel to the growth direction. Thereby, the azimuthal cut direction was approximately along the <112> direction through the edge facets of the growth ridge for the FZ experiments, while for the ZM experiments its direction was arbitrary. The slices were subsequently prepared by grinding, polishing, and Secco etching. Optical microscopy was used to analyze the facets by the procedure described in more detail in [23,30]. In addition, the dislocations in the samples were studied by XRT measurements (transmission).

In total 31 FZ crystals and 41 ZM crystals were grown and analyzed in the present work.

3. Results

3.1. FZ experiments in the double-ellipsoid mirror furnace with necking

Fig. 2a) shows the cross section of a Si crystal grown at 33 μm s^{-1} in the double ellipsoid mirror furnace. The cut neck is on the left of the picture (cf. also Fig. 1). Then, a diameter increase followed, with the lamp powers adjusted to keep a constant diameter. Interface destabilization, due to constitutional supercooling because of segregation of the As dopant, can be seen on the right side and occurred when the lamp power was decreased and the growth velocity increased [23]. Due to imperfect radial symmetry in the temperature field, the 10 rpm rotation produced periodic marks in the crystal that appeared very useful to visualize the interface shape – some are indicated on the picture – as well as the (111) central facet occurring perpendicular to the axis of the sample. Fig. 2c) is a plot of the variation of the facet diameter along the sample length. The facet occupied almost the full diameter of the neck, then increased a lot in the shouldering part, in relation with a decrease of the interface curvature, after which a steady state, in terms of growth rate, interface curvature and facet diameter (4.2 mm), was reached. Another flattening of the interface, at the end of pulling, produced another increase of the facet diameter.

In all the experiments analyzed in this paper, biased facet diameter measurements occurred, because of unavoidable misalignment of the facet center with the cutting plane. This was either due to inaccurate cut or to distance from the center of the facet to the sample axis. This uncertainty was in the range of a few tenth of millimeter but could reach one millimeter in certain cases.

The interface radius of curvature varies from 5 mm to 20 mm and is strongly dependent on the experiment, with an apparent increase with pulling rate. While all samples present the same facet evolution, the diameter values are different because of these differences in interface curvature.

Fig. 2b) shows an X-ray topograph of the 1.5 mm thick slice cut along

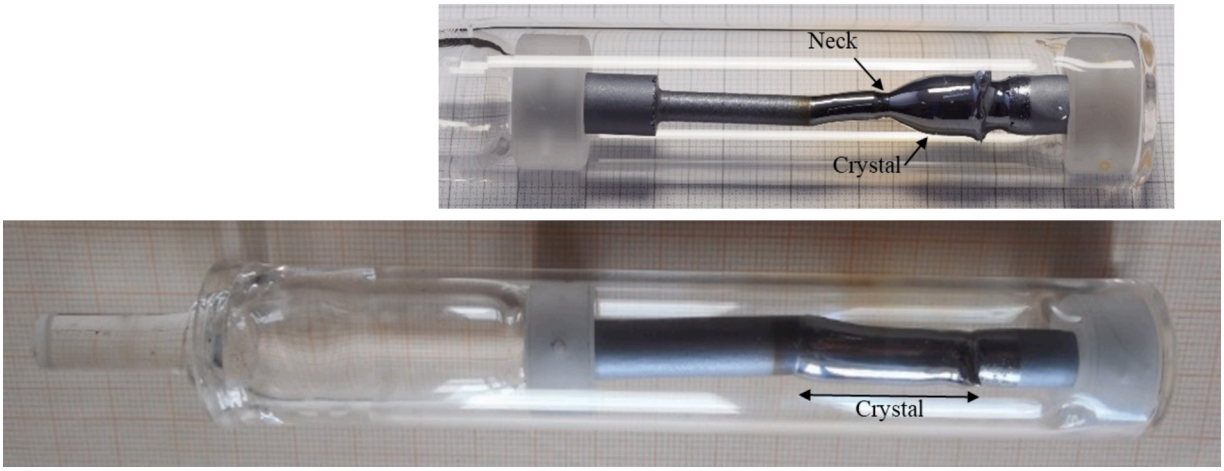

Fig. 1. View of growth ampoules after experiments in the double-ellipsoid mirror furnace MHF, with neck (top), and in the mono-ellipsoid mirror furnace ELLI (bottom). Growth proceeded from left to right and grown samples are 8 mm in diameter.

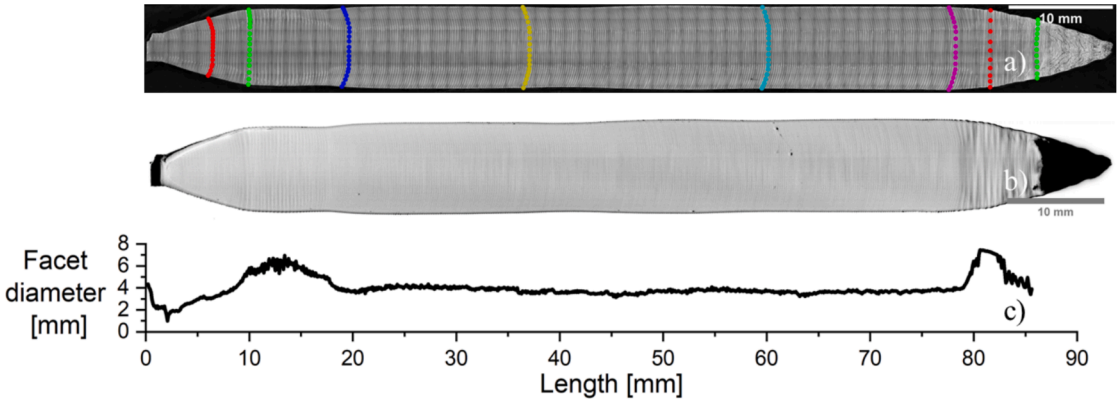

Fig. 2. a) Cross section of an etched Si crystal grown in the double ellipsoid mirror furnace at 33 μm s^{-1} Growth occurred from left to right. Colored dotted lines represent various interface shapes. b) X-ray transmission topograph of a cross section of the same crystal. c) Variation of facet diameter as function of sample length.

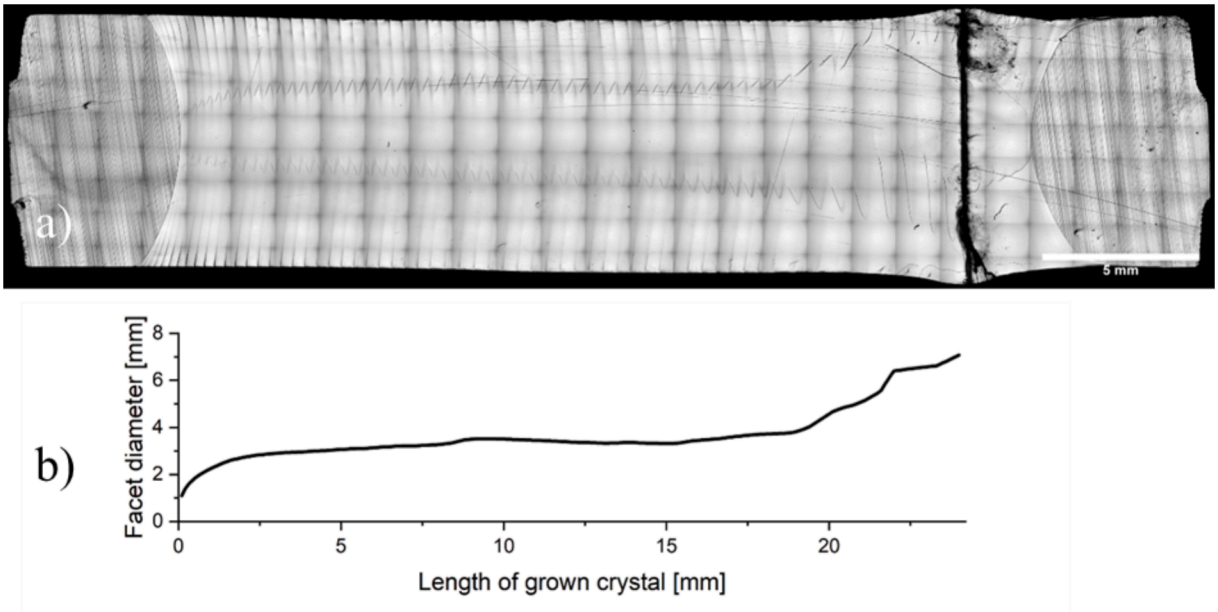

Fig. 3. a) Cross section of an etched Si crystal grown in the monoellipsoid mirror furnace at 80 μm s^{-1} Growth occurred from left to right. b) Variation of facet diameter as function of sample length.

the sample axis. The crystal is almost entirely free of dislocations, only in the finally solidified part a high density of dislocations is observed. The absence of dislocations indicates that the facet growth kinetics follow the 2D nucleation dynamics.

3.2. ZM experiments in the mono-ellipsoid mirror furnace with high pulling rate

These experiments occurred under O_2 atmosphere to ensure the stability of the SiO_2 layer on the surface, which was generated on the silicon rod before the growth experiment, to prevent Marangoni convection. The zone melting setup with a fixed relation between seed and feed rod made it impossible to do necking so that the samples directly began with the seed diameter, 8 mm.

Fig. 3a) shows the etched surface of a sample cut along its axis. The hatched areas on both sides are the unmolten parts of the initial sample. Here also, rotation striations allowed the observation of the interface curvature and facet length. The solid–liquid interface was strongly curved at the beginning of the pulling. Then growth rate increased, as it can be seen from the increasing distance between striations, and curvature decreased until it reached a stable shape. Decreasing the lamp power at the end of the experiment produced an increase of the growth rate and flattening of the interface. As it can be seen on Fig. 3b), a facet appeared immediately at the beginning of pulling and its diameter increased with simultaneous increase of growth rate and decrease of curvature. Then the facet diameter stabilized to 2.5 mm until it increased again at the end.

All samples processed at pulling rates larger than 16.6 μm s^{-1} show the same stable facet diameter behavior, with values ranging from 1.7 mm for a pulling rate of 33 μm.s^{-1} to 2.5 mm for a pulling rate of 80 μm s^{-1}, with one exception, which will be discussed in chapter 4.1.3.

3.3. Mono-ellipsoid mirror furnace with 16.6 μm s^{-1} pulling rate

Fig. 4 shows that samples grown at the lowest pulling rate had a different behavior in terms of facet diameter. While a few have a stable diameter (such as ELLI-1), others (ELLI-2 to ELLI-4) show a plateau followed by an increase of the facet diameter with subsequent strong fluctuations, or even strong fluctuations without visible plateau (ELLI-5). Fig. 5 emphasizes sample ELLI-4. The facet did not appear immediately at the beginning of the growth (Fig. 5a), which is attributed to misalignment between the facet center and the cutting plane. After a plateau at a level of 0.8 mm, the facet diameter began to increase after 12 mm of growth and finally oscillated with values in the range 0.5 mm to 2.5 mm (Fig. 5c). Cut misalignment probably gives underestimated values. The beginning of the facet diameter increases and the growth phase with facet fluctuations corresponds to an improvement of the structural quality of the crystal, as it can be seen on the x-ray topography in Fig. 5b.

The analysis of the results obtained on 12 samples led to the conclusion that all samples follow a general pattern:

- An initial plateau with a facet diameter of about 1.5 mm, which can extend all along the sample (ELLI-1) or only at the beginning (ELLI-5, apparently masked by misalignment).
- Then an increase of the facet diameter followed by fluctuations, where the amplitudes increase with the grown length and can reach 3.5 mm.

No correlation between the diameter pattern characteristics (plateau length, maximal and minimal facet diameters, frequency of fluctuations) exists with the recorded process parameters such as lamp power, molten zone size or shape, pulling rate or interface curvature. However, most samples show a general increase of quality with length on the X-ray topographs.

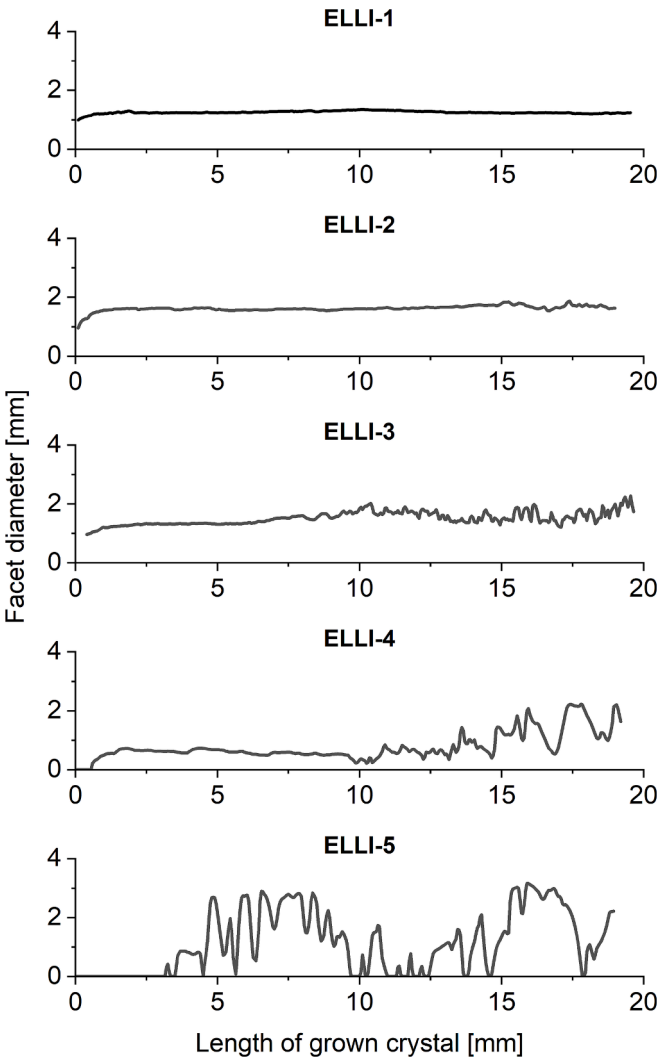

Fig. 4. Facet diameter fluctuations along the length of five crystals grown in the ELLI mono-ellipsoid mirror furnace at 16.6 μm s^{-1} Growth proceeded from left to right.

3.4. Measurement methodology

The discussion in the last part of this paper uses measurements of experimental undercooling and facet velocity. Fig. 6 shows how they proceed from the micrograph of an etched cross section obtained at the beginning of a sample grown in the ELLI mono-ellipsoid mirror furnace. Oscillations of the facet are due to the misalignment of the sample rotation axis with the mirror focal point. The time interval Δt (s) between two striations is obtained from the rotation rate *rpm*:

$$\Delta t = \frac{60}{rpm} \tag{6}$$

and the velocity of the facet, V_F (μm s^{-1}), from the difference of positions between two facet oscillations, Δx_F:

$$V_F = \frac{\Delta x_F}{\Delta t} \tag{7}$$

Visually adjusting a circle on the closest striation gives the radius of curvature R of the rough (i.e. non-facetted) interface. Following the method explained by Brice [31], the facet undercooling ΔT_F is calculated from the facet diameter D_F, with the improvement of using the mean temperature gradient $\overline{\nabla T}$:

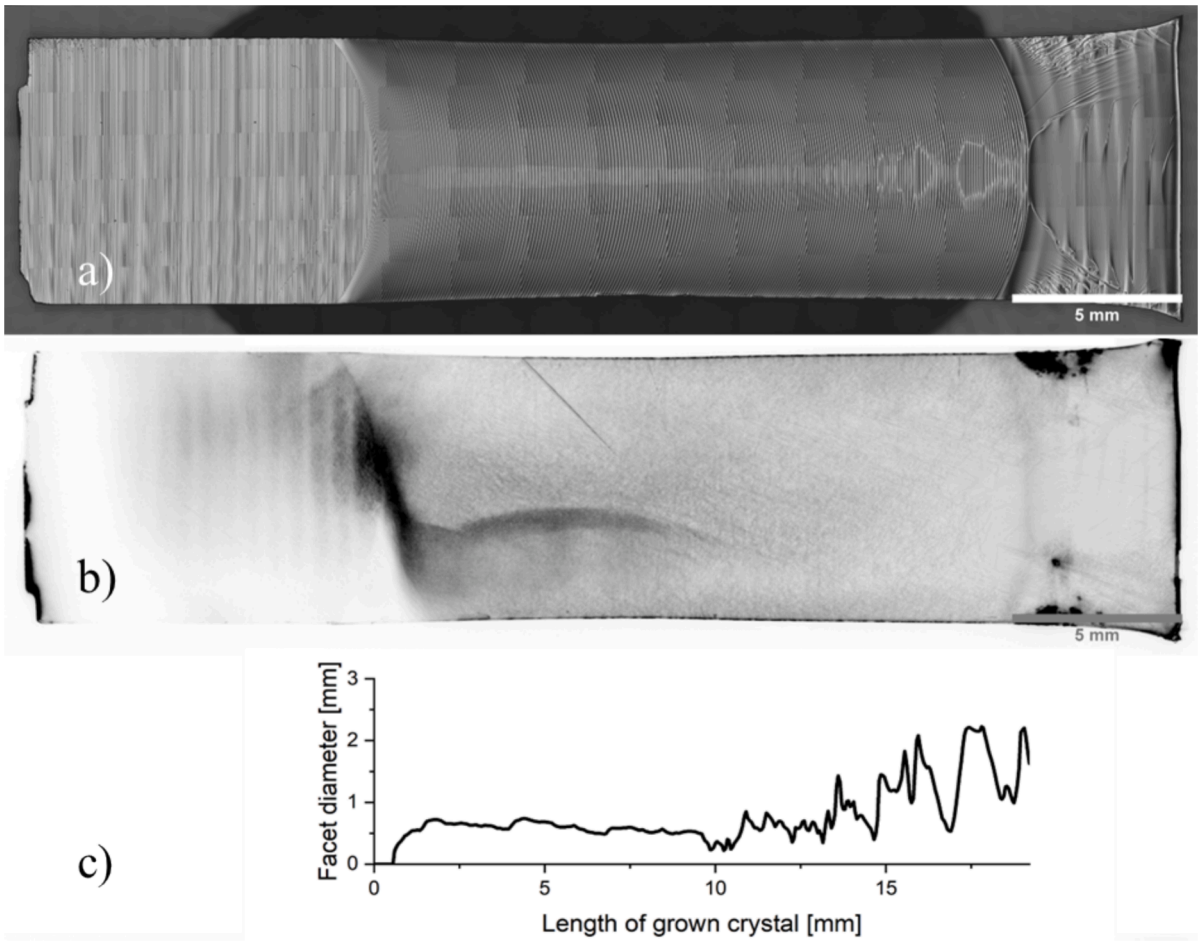

Fig. 5. a) Cross section of sample ELLI-4 grown at 16.6 µm s^{-1} Growth occurred from left to right. b) X-ray topograph of a 1.5 mm thick slice cut on the axis. c) Variation of facet diameter as function of sample length.

$$\Delta T_F = \overline{\nabla T}\left(R - \sqrt{R^2 - \left(\frac{D_F}{2}\right)^2}\right) \tag{8}$$

This mean temperature gradient considers the fact that the volume between the facet and the melting isotherm (supposedly unaffected by the facet) is liquid and not solid. Voronkov [14] derived the value of the mean temperature gradient:

$$\overline{\nabla T} = \frac{k_s \nabla T_s + k_l \nabla T_l}{k_s + k_l} \tag{9}$$

with k_s and k_l are the thermal conductivities of solid and liquid. Its computation from the gradient in the solid ∇T_s (l is for liquid) takes into account the heat balance at the solid–liquid interface, with ΔH the solidification enthalpy per unit volume:

$$k_s \nabla T_s = k_l \nabla T_l + \Delta H V_F \tag{10}$$

Measurements of the facet position difference Δx_F have an accuracy better than 20 µm and the rotation rate was constant, so that, in principle, the velocity accuracy should be better than 5 %. However, as will be seen on Fig. 9, dispersion is higher, probably due to fluctuations of the interface response to the rotating temperature field. Facet diameter measurements are precise but contain the above-mentioned error due to the deviation of the sample surface from the crystal center. The undercooling accuracy depends also on the temperature gradient, discussed in the following, and on the radius of curvature measurement, the accuracy of which is 5 %. Anyhow, measurements at constant growth rates show a 15 % variation of the undercooling, for a given gradient, which looks acceptable.

4. Discussion

4.1. Temperature gradient and kinetic laws

4.1.1. Crystals without dislocation

Because the FZ grown crystals begin with a neck, it is not possible to perform measurements of growth rate increase for these samples. Only measurements during steady state, i.e. constant striation periodicity, are possible. As the samples are dislocation-free in the main growth region as verified by XRT measurements, the facet kinetic is of the 2D-seed nucleation type, i.e. it follows the Eqs. (1) to (3). In order to conclude for a given kinetic law, the measured undercooling should be compared to the undercooling computed for the given growth rate. However, the undercooling depends on the temperature gradient in the sample. This is around 100 to 150 K cm^{-1} as discussed in the next paragraph. Table 1 shows eight results obtained for four samples. Thanks to a good enough etching contrast, MHF-2 and MHF-3 were measured at four and two positions along the axis, respectively. The interface radius of curvature R varies significantly from one sample to another and inside a sample, most likely due to the evolution of the geometry of the molten zone and the sample motion relative to the mirrors. The three kinetic equations give the undercooling values expected for the given pulling rate. From these values and from the measured radius of curvature and facet diameter, reversing Eq. (8) and using Eqs. (9) and (10) gives the corresponding temperature gradient in the solid.

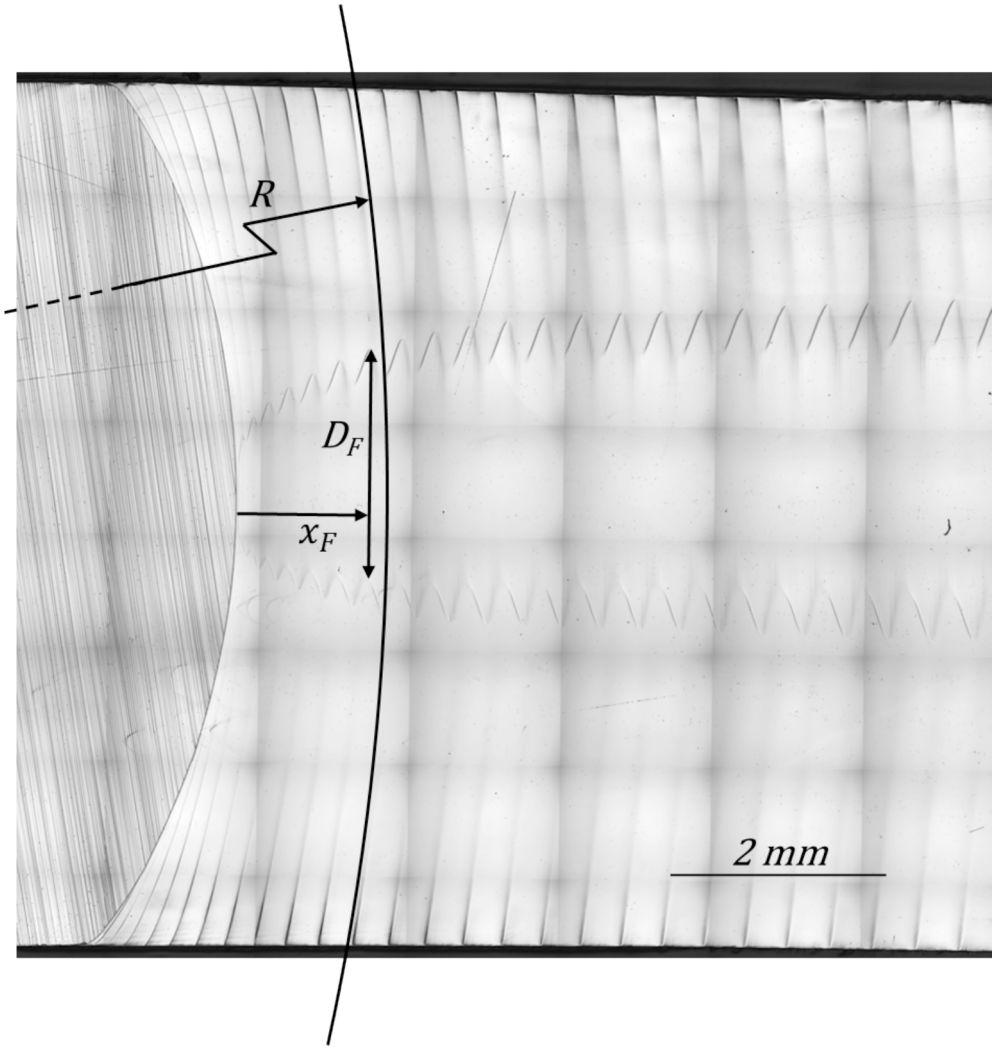

Fig. 6. Measurements of facet position (x_F), facet diameter (D_F) and interface radius of curvature (R) at the beginning of the growth of the sample shown on Fig. 3. The origin of distance is at the beginning of the growth, on the un-molten seed interface.

Table 1
Temperature gradients in the solid obtained from the measurements of interface curvatures and facet diameters of four samples pulled in the MHF double-ellipsoid mirror furnace.

Sample	Pulling rate (μm.s^{-1})	R curvature (mm)	Temperature gradient in solid (K.cm^{-1})		
			Equ. (1)	Equ. (2)	Equ. (3)
MHF-1	16.6	5	258	326	105
MHF-2-a	33.3	11	303	387	125
MHF-2-b		9	195	249	81
MHF-2-c		10	305	390	126
MHF-2-d		5	347	443	143
MHF-3-a	66.6	11	250	324	105
MHF-3-b		25	319	414	135
MHF-4	50	12	350	449	146

The Eq. (3), obtained through molecular dynamic simulation [16], gives reasonable temperature gradients in the solid, in the expected range. It thus should be favored for kinetic calculations of faceting in Si single crystals without dislocation. The gradients vary significantly, even during the growth of one sample, likely because of the already mentioned geometrical changes.

4.1.2. Samples with dislocations

As seen on Fig. 6, the samples grown in the ELLI mono-ellipsoid mirror furnace without neck show an increase of velocity and facet size at the beginning of the growth. Therefore, it is possible to measure the undercooling as function of the facet growth rate. Measurements on seven samples gave parabolic plots, as expected from the presence of dislocations in these samples (see Eq. (4)). As the kinetic law in case of dislocation interaction must be the same for all experiments, all data should fit to a single parabolic curve. For complying to this requirement, the temperature gradients have been adjusted, for each experiment, with respect to values obtained by numerical simulation [22]. As shown on

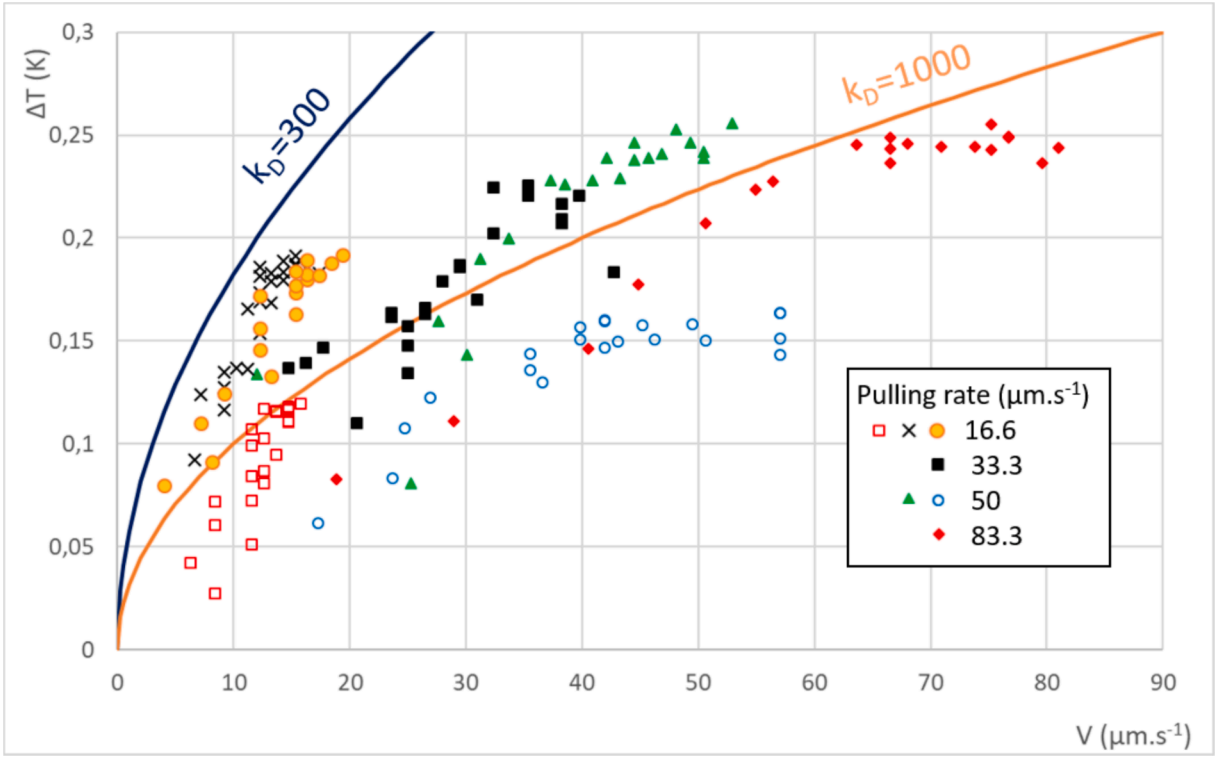

Fig. 7. Plot of undercooling ΔT as function of growth rate V, at the beginning of seven experiments performed in the ELLI mono-ellipsoidal mirror furnace. The solid lines represent the Eq. (4) with the two coefficients available in the literature.

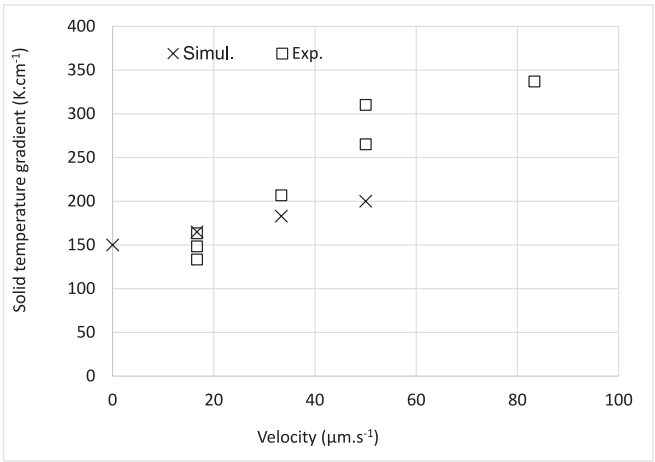

Fig. 8. Adjusted temperature gradients in the solid for the seven experiments plotted on Fig. 7 and results of numerical simulation of heat transfer in the ELLI furnace.

Fig. 7, the agreement is better with a kinetic coefficient $k_D = 1000$ μm.s^{-1}.K^{-2} [18].

Fig. 8 shows the chosen temperature gradients in the solid as function of pulling rate, as well as temperature gradients obtained through numerical simulation of heat transfer in the ELLI furnace [23]. The agreement is reasonably good, while simulation underestimates the increase of gradient with pulling rate.

4.1.3. Sample with sudden increase of facet diameter

Fig. 9a shows the etched surface of the sample giving open blue circles on Fig. 7. Contrarily to all other samples grown at velocities larger than 16.6 μm s^{-1}, it shows a large increase of facet size, after 7 mm of growth. The x-ray topograph (Fig. 9b) shows that this corresponds to a decrease of the dislocation density, followed by dislocations organized along slip lines.

Fig. 9c) plots the measured undercooling as function of velocity, at the beginning of growth and in the large facet area. While the beginning fits well to the dislocation driven kinetic law, for the temperature gradient adjusted to 180 K cm^{-1}, it appears that the large facets show undercooling in good agreement with Eq. (3), i.e. no dislocation perturbation of the facet. This is contradictory to the dislocations observed on the x-ray topograph. An explanation could be that the number of dislocations decreased suddenly, for an unknown reason, so that the facet kinetic changes from dislocation-driven to the 2D seed nucleation case. The dislocations visible in the x-ray topograph in this area would have then been created after growth, during cooling down due to the rather high temperature gradient, as suggested by their organization along slip lines. Hence, the gradient adjusted for the dislocation-driven case at the beginning of growth gives a good agreement with the 2D-seed nucleation kinetic for the subsequent growth; this is another argument for favoring Eq. (3).

4.2. Modeling dislocation-facet interaction

As observed in the previous section, the x-ray topographs should be taken cautiously as they show the sample structure after cooling down, when dislocations might have multiplied. Anyhow, due to thermal stresses during the heating and without necking, the dislocation density was certainly high at the beginning of the growth in the mono-ellipsoidal mirror furnace. At the end of growth, the number of dislocations affecting the facet was certainly lower than observed on the post-cooling topographs. Dislocations in the samples grown at low velocity might be a cause for the strong fluctuations of facet diameter observed in these samples. This would mean that higher dislocation densities, at the beginning, produce a constant facet diameter, in agreement with the parabolic relationship obtained on Fig. 7. Later on, the dislocation density decreases, possibly leading to individually distinct dislocation-facet interactions producing facet velocity and then facet diameter

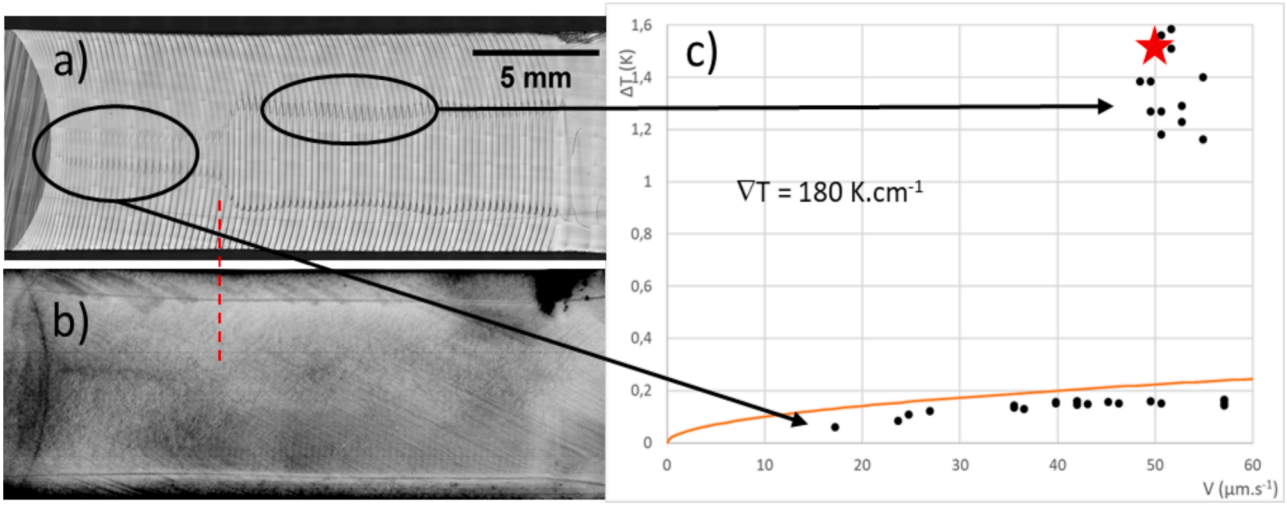

Fig. 9. A) etched surface of a sample grown in the elli furnace. b) corresponding x-ray topograph. c) Measurements of undercooling and velocity at the beginning of growth (already shown on Fig. 7) and in the large facet area. The solid line represents Eq. (4) and the star Eq. (3).

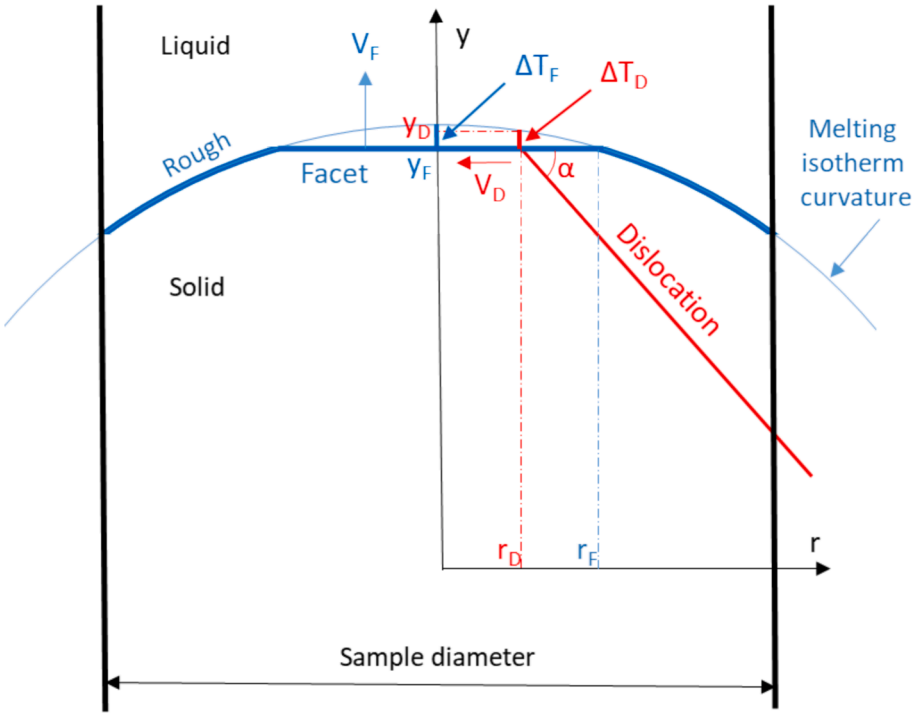

Fig. 10. Geometrical model for calculation of dislocation-facet interaction.

fluctuations. The geometrical model presented on Fig. 10 has the objective to check this hypothesis.

The whole system is axi-symmetric with a constant radius of curvature R of the rough interface. The r and y axes are linked to the uniform movement of the rough interface, which grows upwards at the stationary rate V_{pulling}. During the initial steady state, V_{pulling} and Eq. (3) give the facet undercooling ΔT_F. A mean temperature gradient $\overline{\nabla T}$ is set, from which Eq. (8) gives the facet diameter D_F. The facet position y_F is computed from the simple geometrical relation:

$$y_F = R - \frac{\Delta T_F}{\overline{\nabla T}} \tag{11}$$

The mechanism of interaction of a dislocation with a facet has been described in detail, while qualitatively, by Voronkov and Pankov in 1974 [32]. Their approach is developed in a quantitative model, taking into account the kinetic coefficients derived in the previous paragraphs. The model begins with the dislocation tip impinging the border of the facet, at radius $r_D = r_F$ and at angle α. For a 60° dislocation this angle α with the (111) plane is 54.7°. Dislocations are aligned on <110> directions, which gives a linear trajectory of the impinging point on the facet surface. This trajectory may pass through the facet center, which is the case described here for simplicity. It might also pass away from the center, which requires some equation modifications in order to compute properly the undercooling at the dislocation tip. The model does not consider additional lateral glide of the dislocation due for example to mechanical stresses. When growth proceeds, the dislocation tip moves radially towards the facet center with a velocity:

$$V_D = \frac{V_F}{\tan(\alpha)} \tag{12}$$

The model proceeds with successive time steps t_i for a constant time interval Δt. The main hypothesis in the model is that, at each time, the facet grows with a velocity that is the largest one, between the 2D-seed kinetic – Eq. (3) using ΔT_F – and the dislocation kinetic – Eq. (4) using the dislocation tip undercooling ΔT_D (Fig. 10). Knowing the state of the system at time t_{i-1} (i.e. $y_{F,i-1}$, $V_{F,i-1}$, $r_{D,i-1}$) the following set of equations gives the new state at time t_i:

$$\begin{aligned}
&\text{Facet undercooling}: \Delta T_{F,i} = \left(R - y_{F,i-1}\right)\overline{\nabla T},\\
&\text{Radius at dislocation tip}: r_{D,i} = r_{D,i-1} + \frac{V_{F,i-1}}{\tan(\alpha)}\Delta t,\\
&\text{Isotherm above the dislocation tip}: y_{D,i} = \sqrt{R^2 - r_{D,i}^2},\\
&\text{Undercooling of dislocation tip}: \Delta T_{D,i} = \left(y_{D,i} y_{F,i-1}\right)\overline{\nabla T},\\
&\text{Facet velocity}: V_{F,i} = Max\left[V_{0D}(\Delta T_{F,i}),\ V_{dislo}(\Delta T_{D,i})\right],\\
&\text{Facet position}: y_{F,i} = y_{F,i-1} + \left(V_{F,i} - V_{pulling}\right)\Delta t,\\
&\text{Facet radius}: r_{F,i} = \sqrt{R^2 - y_{F,i}^2},
\end{aligned} \tag{13}$$

Then, the process repeats until the dislocation passed the entire facet. Plots of facet diameter as function of grown length ($= V_{pulling} t_i$) will show the results. Some numerical instabilities come from the calculation of $\Delta T_{F,i}$ and $\Delta T_{D,i}$, which should more correctly proceed from $y_{F,i}$, so that time steps $\leq$0.5 s should be used.

4.3. Simulation results

The common set of parameters used for the simulations is: Eq. (3) for $V_{0D}(\Delta T_F)$, $k_D = 1000\ \mu m\ s^{-1}\ K^{-2}$ for $V_{dislo}(\Delta T_D)$, $\overline{\nabla T} = 100$ K.cm^{-1}, $R = 12$ mm, $V_{pulling} = 16.6\ \mu m\ s^{-1}$ and $\alpha = 54.7°$.

4.3.1. One dislocation

When the dislocation tip is within 120 μm from the facet border, its undercooling is small, and the facet keeps on growing with 2D-seed kinetic (Fig. 11a)). Later, the dislocation-driven kinetic results in a larger facet velocity, which increases fast as the dislocation tip moves towards the facet center (Fig. 11b)). This large facet velocity produces a decrease of the distance to the melting isotherm, so that the undercooling and the facet velocity decrease. Then, the dislocation tip passes the facet center, where facet velocity reaches the pulling rate. Later, the undercooling still decreases, until the receding of the facet, relatively to the melting isotherm, increases the undercooling, and the facet velocity increases quickly to reach the pulling rate. As expected, a smaller curvature of the interface (Fig. 11c)) as well as an increase of temperature gradient (Fig. 11d)) result in a decrease of the overall facet diameter. Modification of the pulling rate also results in corresponding diameter changes, so that it appears that this simple geometric model catches the physics of the dislocation-facet interaction. Dislocations crossing the facet on other lines, away from the facet center, show the same behavior as Fig. 11, but with a smaller effect on the facet diameter. For example, the perturbation due to a dislocation crossing the facet 1.2 mm away from its center, only extends on 3.5 mm of growth and gives a minimum facet diameter of 2600 μm.

It is remarkable that the facet size evolves between 3.6 mm and 1.1 mm, which are values close to the experimental maximum and minimum of the facet diameter (see chapter 3.3). This argues in favor of dislocations acting as sources of the observed facet diameter fluctuations, with the plateau integrating the effect of numerous dislocations, while a decreasing dislocation density results in dislocations acting independently, with large diameter fluctuations.

4.3.2. Ten dislocations

The effect of dislocation density variations is studied with sending ten dislocations with a given periodicity through the facet. Simulations proceed in the same way than with one dislocation. In case of several dislocations affecting a facet, it is generally admitted that one disloca-

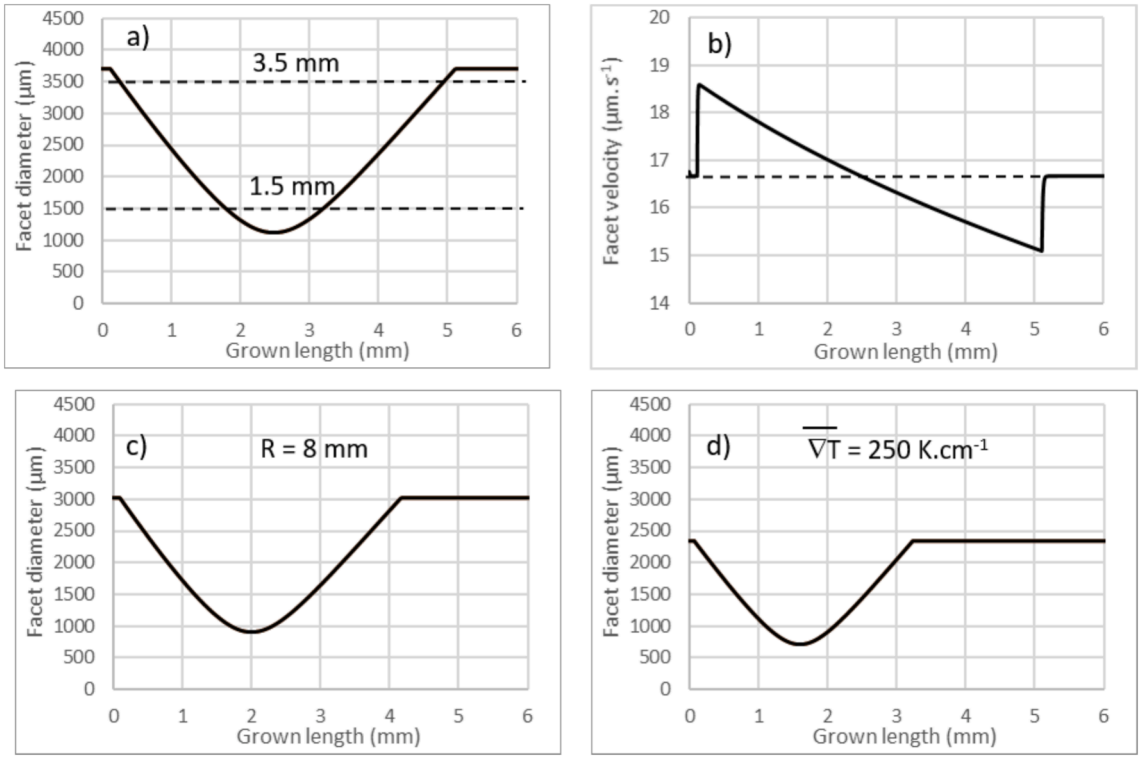

Fig. 11. Computed facet diameter (a) and velocity (b) changes when a single dislocation crosses the facet through its center, as function of the length of crystal grown since the beginning of the dislocation-facet interaction. Effect of a smaller interface radius of curvature (c) and of a larger temperature gradient (d).

tion expands its steps on top of the others and then is the only source of steps. The model presented here follows this assumption, with the further hypothesis that this dislocation is the one that has the largest undercooling at its tip. Hence, the leading dislocation may change from one to another, depending on the evolution of their tip undercooling on the facet surface. Consequently, the facet velocity is chosen as the largest one, between $V_{0D}(\Delta T_{F,i})$ and the ten $V_{dislo}(\Delta T_{D,i})$.

Preliminary simulations have shown that dislocations passing close to the center of the facet screen the effect of other dislocations crossing the facet outside the center. This is because the quadratic kinetic law enhances the effect of the larger undercooling of the centered dislocations. Therefore, the effect of a two-dimensional dislocation network (EPD) can be modeled by considering only a line of dislocations that crosses the center of the facet. Hence, ten dislocations are sent towards the center of the facet with a given periodicity, Π, of the order of the square root of the dislocation density, from $\Pi = 100\,\mu m$ (EPD $10^4\,cm^{-2}$) to $\Pi = 3200\,\mu m$ (EPD $10^1\,cm^{-2}$). Results are shown on Fig. 12a) to Fig. 12c). When the dislocation density is large, the individual effects of the dislocations on the facet diameter merge into a constant value at 1.1 mm, which accounts satisfactorily for the plateau observed on all samples studied in chapter 3.2 and 3.3. Decreasing the dislocation density results in fluctuations of the facet diameter with increasing amplitude and period. This also accounts for the observations performed on samples grown at $16.6\,\mu m\,s^{-1}$, where the X-ray topographs show a gradual decrease of dislocation density (Fig. 5c), simultaneously to an increase of facet diameter fluctuations period and amplitude (Fig. 5b). It is hypothesized that the fact that facet diameter fluctuations do not occur in samples grown at higher pulling rate (see chapter 3.2), is related to the increase of temperature gradient with pulling velocity (Fig. 8) leading to higher stresses in the crystal and, hence, a larger multiplication of dislocations.

Results on Fig. 12c) reflect correctly the amplitude of facet diameter fluctuations, but they show a period of 5 mm, while the experimental period, for the largest peaks, is rather in the 1 mm range (Fig. 4, sample ELLI-5). This is linked to the long time taken by the dislocation to cross the entire facet at the velocity V_D (equation (12)). In-situ synchrotron observation [33] suggested that 60° dislocations are unstable at the growth interface, especially in case of undercooling, and that common dislocations show no effect on the facet growth, contrarily to composite dislocations. This author also reports that "<001> dislocations often exist along the center axis of a bulk crystal". Such dislocations have an angle of 35° to the (111) plane. Using molecular dynamic simulation, Zhou [34] shows that, during growth below a (111) plane, the growth dislocations slip on the (111) <112> system, inclined at 28.1° to the facet plane. While such dislocations are not commonly reported in literature, their lower angle would result in a faster crossing of the facet and then shorter period of facet fluctuations (Fig. 12d), in better agreement with the experiments.

However, other in-situ X-ray observations of Si growth [35] show 60° dislocations but moving perpendicularly to the interface, in agreement with similar published results [36]. This would result in much longer crossing time; indeed, the dislocation would stay at the facet border. However, the video attached to this paper [33] shows that it takes about 30 s for this alignment, so that a significant angle may exist in practice. Furthermore, it also appears that the dislocations, while they are perpendicular to the interface, drift laterally (estimated at $0.1\,mm\,min^{-1}$ from the video), which is attributed by the authors to stress acting on the sample. This would be a reasonable cause of decreasing the time needed to cross the facet.

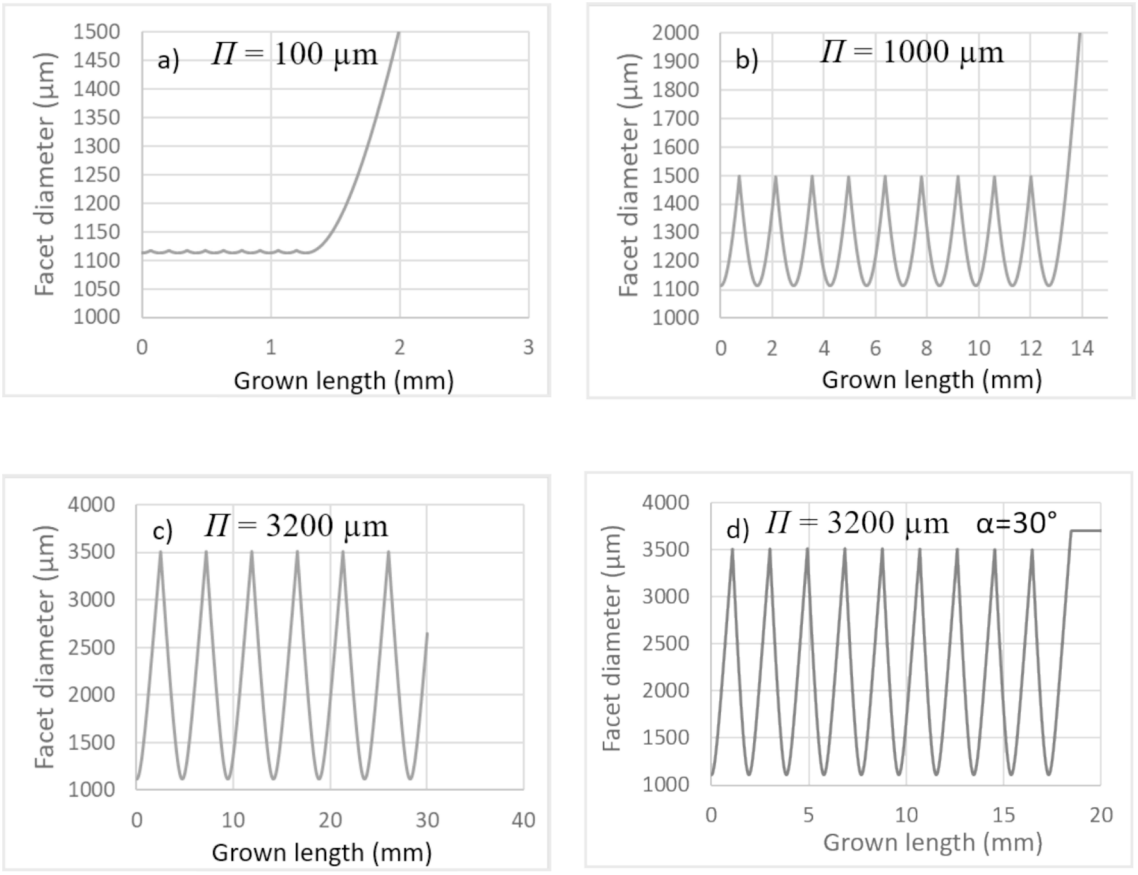

Fig. 12. Fluctuations of facet diameter with grown length, when ten dislocations are crossing the center of the facet, with various periodicities, a) to c). Effect of decreasing the angle between the dislocation line and the facet plane.

5. Conclusion

All silicon samples grown in the <111> direction have shown facets perpendicular to the growth axis. Experimental undercooling-velocity relationships show that the facet kinetics belong to the 2D-seed mechanism for samples without dislocations, or to the dislocation driven mechanism for the other samples. These measurements allowed identifying the most reasonable kinetic coefficients for both cases, among the various values available in the literature.

An interesting case appeared for dislocated samples grown at low pulling rate under smaller temperature gradients. This resulted in a decrease of the dislocation density along the samples. Simultaneously, increasing facet diameter fluctuations are observed. A simple geometric model, using the kinetic coefficients derived here above, suggests that the facet diameter might have evolved from a stable small value for high dislocation density, to a fluctuating diameter showing the effect of individual dislocations when their density decreases. The lower the dislocation density, the larger the diameter fluctuations. Therefore, interaction of individual dislocations may generate the observed facet diameter fluctuations. However, the dislocation density at the interface during the growth of these crystals is unknown, so that this dislocation-facet interaction remains hypothetical. In order to check this hypothesis, in-situ observation (e.g. in-situ X-ray topography) of dislocation-facet interactions is proposed.

CRediT authorship contribution statement

Christian Kranert: Writing – review & editing, Project administration, Conceptualization. **Paul Wimmer:** Investigation, Data curation, Conceptualization. **Jochen Friedrich:** Writing – review & editing, Supervision. **Thierry Duffar:** Writing – original draft, Investigation, Formal analysis, Data curation.

Declaration of competing interest

The authors declare the following financial interests/personal relationships which may be considered as potential competing interests: [Christian Kranert reports financial support was provided by German Aerospace Center DLR. Christian Kranert reports financial support was provided by Federal Ministry for Economic Affairs and Climate Action. Thierry Duffar reports financial support was provided by Bavarian Research Foundation. If there are other authors, they declare that they have no known competing financial interests or personal relationships that could have appeared to influence the work reported in this paper].

Acknowledgements

This research was funded by the DLR/BMWK under FKZ 50WM1844/50WM1845 and FKZ 50WM2144/50WM2145. The former colleagues Dr. Tina Sorgenfrei and Dr. Thomas Jauss of the Institute for Earth and Environmental Sciences of the Albert-Ludwigs-University in Freiburg, Germany are gratefully acknowledged for performing the FZ and ZM experiments and carrying out part of the characterization of the grown crystal presented in this work. Thierry Duffar is very grateful to the Bayerische Forschungsstiftung for supporting his stay at the Fraunhofer IISB with the FACET PIZ-240-24 grant.

Data availability

Data will be made available on request.

References

[1] M. Jurisch, S. Eichler, M. Bruder, Vertical Bridgman Growth of Binary in Compound Semiconductors, Elsevier, Amsterdam, The Netherlands, 2015, pp. 331–372.
[2] T.P. Chen, F.R. Chen, Y.C. Chuang, Y.D. Guo, J.G. Peng, T.S. Huang, L.J. Chen, J. Cryst. Growth 118 (1–2) (1992) 109–116.
[3] H. Koh, M. Choi, I. Park, T. Fukuda, Cryst. Res. Technol. 30 (1995) 397–403.
[4] H. Chung, M. Dudley, D. Larson Jr., D. Hurle, D. Bliss, V. Prasad, J. Crystal Growth h 187 (1998) 9–17.
[5] V. Antonov, V. Elsakov, T. Olkhovikova, V. Selin, J. Cryst. Growth 235 (1–4) (2002) 35–39.
[6] V.V. Voronkov, Izv. Akad. Nauk, Ser. Fiz. 49 (12) (1985) 2467–2472.
[7] T. Abe, J. Growth 24–25 (1974) 463–467.
[8] L. Stockmeier, L. Lehmann, A. Miller, C. Reimann, J. Friedrich, Cryst. Res. Technol. 52 (2017) 1600373.
[9] T. Duffar, A. Nadri, C.R. Ac, Sci. Ser. Physique 14 (2013) 185–191.
[10] T. Duffar, A. Nadri, Scipta Mat. 62 (2010) 955–960.
[11] A.A. Chernov, J. Cryst. Growth 24–25 (1974) 11–31.
[12] T. Taishi, Y. Ohno, I. Yonenaga, J. Cryst. Growth 393 (2014) 42–44.
[13] K.A. Jackson, in: Liquid Metals and Solidification, Cleveland, ASM, 1958, pp. 174–186.
[14] V.V. Voronkov, Soviet Phys. – Crystallography 17 (1973) 909–917.
[15] K.M. Beatty, K.A. Jackson, J. Cryst. Growth 211 (2000) 13–17.
[16] V.A. Fabiyi, T. Richmond, B.T. Helenbrook, E. Paek, J. Cryst. Growth 592 (2022) 126736.
[17] W.K. Burton, N. Cabrera, F.C. Frank, Philos. Trans. R. Soc. Lond. 243 (1951) 299–358.
[18] F. Yang, L.C. Chuang, K. Maeda, H. Morito, K. Fujiwara, T. Duffar, J. Cryst. Growth 639 (2024) 127722.
[19] S.S. Mishra, L.C. Chuang, J. Nozawa, K. Maeda, H. Morito, K. Fujiwara, T. Duffar, Scr. Mater. 247 (2024) 116116.
[20] D. Buta, M. Asta, J.J. Hoyt, J. Chem. Phys. 127 (2007) 047703.
[21] W. Miller, J. Cryst. Growth 325 (2011) 101–103.
[22] N. Bagheri-Sadeghi, V.A. Fabiyi, B.T. Hellenbrook, E. Paek, Sensitivity of horizontal ribbon growth to solidification kinetics, J. Crystal Growth 603 (2023) 127038.
[23] S. Gruner, C. Kranert, T. Jauß, T. Sorgenfrei, C. Reimann, J. Friedrich, Crystals 12 (2022) 1575.
[24] A. Eyer, R. Nitsche, H. Zimmermann, J. Cryst. Growth 47 (1979) 219–229.
[25] A. Eyer, A. Cröll, R. Nitsche, J. Cryst. Growth 71 (1985) 173.
[26] P. Dold, K.W. Benz, A. Cröll, B. Roux, D. Lyubimov, T. Lyubimova, R. Scuridyn, Acta Astronaut. 48 (5-12) (2001) 639–646.
[27] W.C. Dash, J. Appl. Phys. 29 (1958) 736.
[28] A. Cröll, W. Müller, R. Nitsche, J. Cryst. Growth 79 (1986) 65.
[29] S. Hürner, J. Friedrich, Public Final Report of the InSituKris-Project founded by DLR under FKZ 50WM1757 (2020).
[30] T. Sorgenfrei, T. Jauß, J. Friedrich, C. Reimann, A. Cröll, Int. J. Microg. Sci. Appl. 34 (1) (2017) 340115.
[31] J.C. Brice, J. Cryst. Growth 6 (1970) 205–206.
[32] V.V. Voronkov and V. M. Pankov, The growth of Si crystals with single dislocations, Kristallografiya 20, 1145-1151, 1974. English translation in Sov. Phys. Crystallogr., 20-6, 697-701.
[33] J. Chikawa, Jpn. J. Appl. Phys. 38 (1999) 4619.
[34] N. Zhou, X. Sui, X. He, S. Huang, L. Zhou, J. Appl. Phys. 125 (2019) 155108.
[35] M.G. Tsoutsouva, G. Regula, B. Ryningen, P.E. Vullum, N. Mangelinck-Noël, G. Stokkan, Acta Mater. 210 (2021) 116819.
[36] B. Ryningen, G. Stokkan, M. Kivambe, T. Ervik, O. Lohne, Acta Mater. 59 (2011) 7703.